Numerical integration method for very high frequencies in the evaluation of Green's functions for layered media: transient wave propagation phenomena

I. Cavalcante[1], J. Labaki[1]

[1]*School of Mechanical Engineering, University of Campinas*
Rua Mendeleyev 200, 13083-860, São Paulo, Campinas, Brazil
i209496@dac.unicamp.br, labaki@fem.unicamp.br

Abstract. This paper is the sequel of a numerical scheme prepared for numerical integration of improper integrals, containing an infinite number of singularities and a decaying tail that oscillates indefinitely. This kind of integrals is common in many engineering unbounded media problems that involve computing Green's functions, which are usually solved with transformed integrals approaches. This work considers the Green's function for case of the time-harmonic response of a multilayered transversely isotropic half-space under external excitations. This response is obtained with the aid the Hankel transform and presented in terms of an exact stiffness matrix method. The solution, in the Hankel transformed domain, was integrated numerically to obtain the corresponding physical domain displacements for very high frequencies. The Fast Fourier Transform (FFT) algorithm was employed in the previously synthesized frequency domain solutions, which results in the determination of transient responses for very small time-steps. The results show that three wave fronts are generated. The displacement velocity of these wave fronts can be associated to compression, shear and Rayleigh waves. This work contributes to our understanding of the numerical evaluation of time-harmonic and transient responses of soil media and is important in many fields of geotechnical engineering and other unbounded media problems.

Keywords: Numerical integration, Green's function, Very high frequency, Countor deformation path, Extrapolation methods of integration

1 Introduction

The frequency of excitation applied in dynamic soil-structure interaction (DSSI) models is usually within the seismic range. Although the response of interest to the DSSI problems is for low frequencies, in order to obtain the transient impulse response of a system through a Fast Fourier Transforms (FFT) algorithm, the implementation must be robust enough to determine the response of this system at very high frequencies [1]. This paper is the sequel of a numerical scheme prepared for numerical integration of improper integrals with respect to the upper limit of integration, containing an infinite number of singularities and a decaying tail that oscillates indefinitely. This kind of integrals is common in the DSSI problems described through boundary element and other meshless methods that involve computing Green's functions, which are usually solved with transformed integrals approaches.

Green's functions for case of the time-harmonic response of a multilayered transversely isotropic half-space subjected to an axisymmetric load on its surface are consider in this work. This response is obtained with the aid the Hankel transform and presented in terms of an exact stiffness matrix method [2]. The stiffness matrix of the layered system is assembled from the stiffness matrix of its constituent layers. The solution, layered system displacements in the Hankel transformed domain, must be integrated numerically in order to obtain the corresponding physical domain displacements [2–4].

To handle the presence of an infinite number of singularities, induced by different wave modes corresponding to body, propagation, reflections and interface waves in the medium [5–8], we use an appropriate contour deformation path for the integration method. This approach enables bypassing the treatment of singularities by simply deforming the contour of integration through a complex half-plane [9–12]. For the oscillatory-decaying part we use a robust series extrapolation through the ϵ-algorithm with selected appropriate endpoints based in the natural

frequency of signal [11–13].

The described methodologies were already applied to investigate the stationary frequency domain solution in previous works [11, 12]. In this paper, this approach is used to evaluate the response at very high frequencies. For this case, the integration scheme must be able to handle the region that would otherwise be dominated by the presence of singularities and is now complicated by a highly-oscillatory behavior. Although the shape of contour deformation path is not critical, its height is restricted by the exponential growth of the Bessel function in the imaginary axis [14]. Alternatively, for very high frequencies the contour should be carefully chosen by shifting the path from the physical poles and branch points, according to [9]. In the sequence, the FFT algorithm was employed in the previously synthesized frequency domain solutions to determine the transient responses for very small time-steps.

These solutions are used to investigate the numerical evaluation of time-harmonic and transient responses of soil media. The influence of the constant hysteretic viscoelastic model considered according to the elastic-viscoelastic correspondence principle [15] is analyzed. The effect of the layer thickness and soil media properties are also addressed.

2 Frequency domain solution

Displacement and stress fields for time-harmonic displacement response of an elastic transversely isotropic N-layered half-space (Fig. 1) subjected to an axisymmetric load have been derived by Labaki et al. [4] from a general expression presented earlier by Rajapakse and Wang [3]. This response is obtained with the aid of the Hankel transform and presented in terms of an exact stiffness matrix method. The radial and vertical displacements $u_i^*(r, z_n)$, $i = r, z$, $n = 1, N + 1$ of the layer interfaces due to radial and vertical loads at arbitrary layers is given in the Hankel transformed domain by

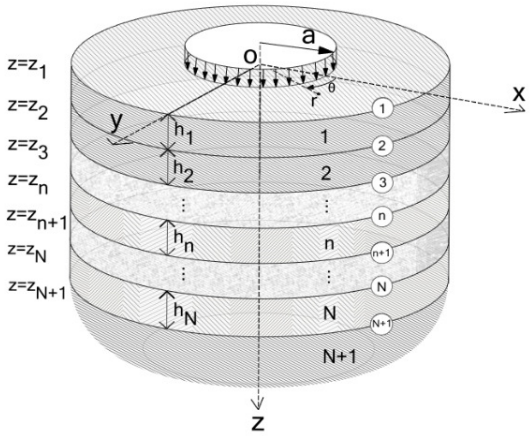

Figure 1. Geometry of layered half-space subjected to an axisymmetric load.

$$\wp^* = Ku^*, \tag{1}$$

in which

$$\wp^* = \left\langle \begin{array}{cccc} \wp_r^{*1} & \wp_z^{*1} & \dots & \wp_r^{*(N+1)} \quad \wp_z^{*(N+1)} \end{array} \right\rangle^T, \tag{2}$$

$$u^* = \left\langle \begin{array}{cccc} u_r^*(r, z_1) & u_z^*(r, z_1) & \dots & u_r^*(r, z_{N+1}) \quad u_z^*(r, z_{N+1}) \end{array} \right\rangle^T. \tag{3}$$

where $\wp^*$ is the vector of external loads applied at the layer interfaces. A vertical disc load of intensity p_0 distributed on an annular area with outer and inner radii s_2 and s_1 can be represented in the Hankel transformed domain by $\wp_{z_n}^{*n} = 1/\zeta[s_2 J_1(\zeta s_2) - s_1 J_1(\zeta s_1)]p_0$, $n = 1, N + 1$, in which J_1 are Bessel functions of the first kind and order 1. The global stiffness matrix (K) of the medium is assembled with the stiffness matrices of each layer [4]. To obtain the displacements at the layer interfaces in the physical domain the solution of displacements from eq. 1 must be integrated according to:

$$u_i = \delta^2 \int_0^\infty u_i^* \zeta d\zeta, \quad i = r, z, \tag{4}$$

where $\zeta = \lambda'/\delta$, in which λ' is the wave number (Hankel space variable) and δ is a normalized frequency of excitation. A detailed expression of global stiffness matrix and all other variables in eqs. (1) to (4) can be found in [12].

2.1 Numerical results in the frequency domain

An important part of this research is the numerical scheme developed to solve eq. 4 yielding accurate solutions for very high values of the excitation frequency. The detailed approach to obtain the frequency solutions can be found in [12]. The Figures 2 and 3 shown respectively, the real and imaginary part of a typical vertical displacement solution resulting from the distributed unit load on the surface of an unbound half-space. The solution was determined at the central point of the loading surface with coordinates $r, z = 0.0$. The loading parameters are $p_0 = 1$, $s_2 = 1$ and $s_1 = 0$. The material properties are $\rho = 1$, $\nu = 0.25$ and Lamé constants $\mu, \lambda = 1$. A constant hysteretic viscoelastic model is considered according to the elastic-viscoelastic correspondence principle [15], with the damping factor $\eta = 0.05$. The frequency solutions given in Figs. 2 and 3 are plotted for the dimensionless frequency parameter $a_0 = \delta a$.

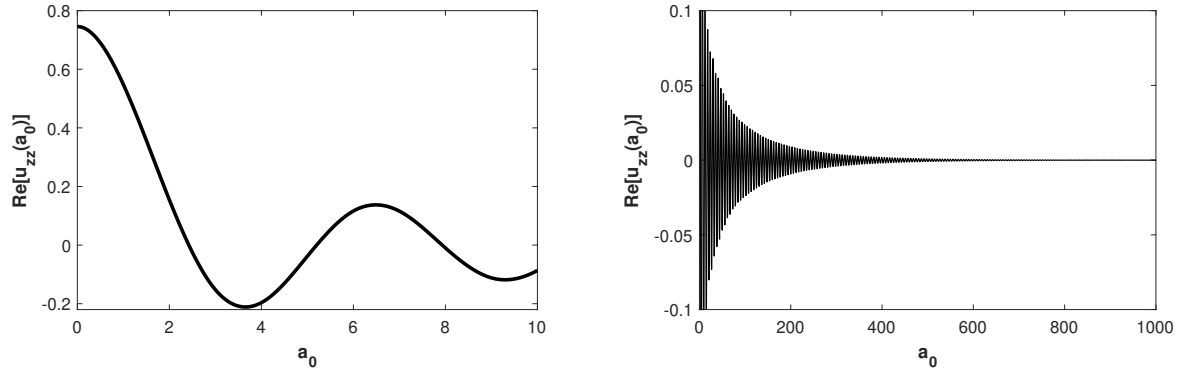

Figure 2. Real part of $u_{zz}(a_0)$ - a) low frequency behavior, - b) high frequency behavior.

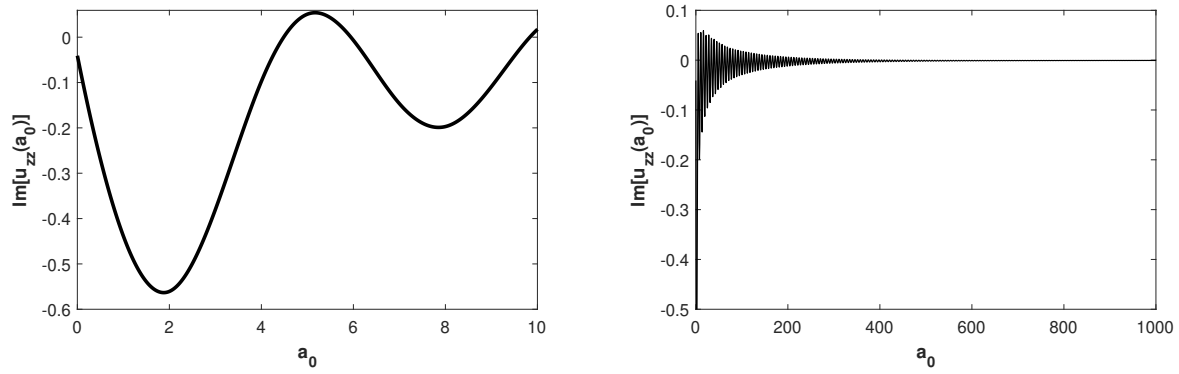

Figure 3. Imaginary part of $u_{zz}(a_0)$ - a) low frequency behavior, - b) high frequency behavior.

Figure 2a shows the real part of the displacement solution for low values of the frequency, while the same solution for very high frequency values is described in Fig 2b. Figure 3a shows the low frequency behavior and Fig. 3b depicts the high frequency content of the imaginary part of the same solution.

3 Transient solutions

The transient solution is obtained by applying the FFT algorithm with respect to the pair (ω,t) to the synthesized frequency domain solutions given in eq. 4. Regarding the Discrete Fourier Transform (DFT) algorithm a relevant issue is the relation between the frequency step $\Delta\omega = \omega_{k+1} - \omega_k$ and the maximum time reachable in the transient process, $T_{max} = 2\pi/\Delta\omega$. Equally relevant is the relation between the time step Δt and the maximum sampling frequency ω_{max} given by $\Delta t = 2\pi/\omega_{max}$ [16]. This implies that the discretization in the time domain of transient phenomena is directly proportional to the sampling frequency for which the original signal is computed. Hence the importance of being able to obtain robust solutions in the frequency domain for very high frequencies such as shown in Figs. 2b and 3b.

Additionally, the signal of the stationary solution which will be investigated must undergo a mathematical treatment as described in [16, 17] prior to being submitted to the FFT algorithm. This mathematical manipulation involves the determination of a cut-off frequency, rules of interpolation to yield smooth transition at the assumed vanishing values above the cut-off frequency and filling the solution with zeros at the high-frequency end of the signal.

4 Numerical results

In this section, three different transversely isotropic materials, whose constitutive parameters c_{ij} are listed in Tab. 1, are considered [18]. Uniformly distributed axisymmetric loads on the surface are considered with fixed values $p_0 = 1$, $s_2 = 1$ and $s_1 = 0$.

Table 1. Transversely isotropic materials used ($c_{ij}^{'} = c_{ij}/c_{44}$).

Material	$\mathbf{c_{11}^{'}}$	$\mathbf{c_{12}^{'}}$	$\mathbf{c_{13}^{'}}$	$\mathbf{c_{33}^{'}}$	ρ
Layred soil[a]	4.46	1.56	1.24	3.26	2.35
Beryl rock	4.13	1.47	1.01	3.62	2.76
Isotropic	3.00	1.00	1.00	3.00	1.00

[a]Limestone/sandstone layered soil.

Initially the results for the numerically synthesized transient responses will be validated considering an elastic isotropic half-space case. In the sequence, the influence of the material, layer thickness and damping parameters on the transient responses for the layered media is investigated.

4.1 Half-space

The previously synthesized frequency domain solutions shown in Figs. 2 and 3 were subjected to the mathematical treatment described in section 3 and to the FFT algorithm. Figure 4a presents the transient vertical displacement response $u_{zz}(t)$ for a long period of time of the point of coordinates $r, z = 0.0$ within the homogeneous half-space. A consistent physical behavior is observed; after a sudden peak, the amplitude of the displacement decreases monotonically towards the zero value of the initial undisturbed solution; on the other hand, there are complex phenomena taking place in the initial time instants (Fig. 4b). As expected, the results show that three wave fronts are generated. These disturbances are clearly recognizable and are due to the arrival of the three waves which propagate in the half-space due to the external loads: compression, shear, and Rayleigh waves, of propagating velocities c_P, c_S, and c_R, respectively. The arrival times of these wave fronts, respectively, $t_P = 0.577$ $[s]$, $t_S = 1.0$ $[s]$ and $t_R \approx 1.088$ $[s]$, are highlighted by dashed vertical lines in Fig. 4b. Notice that the maximum displacement takes place when the Rayleigh waves reaches the observation point. After the passage of the Rayleigh waves the solution decays monotonically.

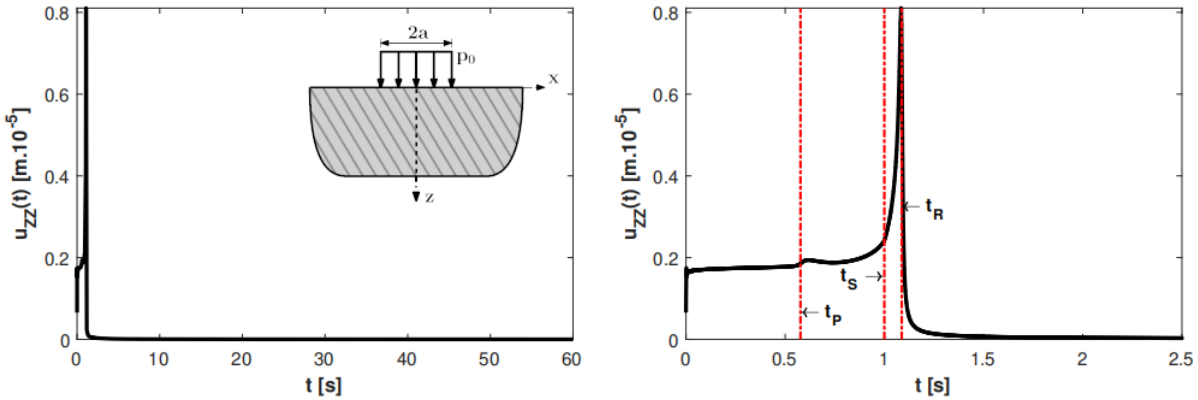

Figure 4. Transient response $u_{zz}(t)$ for - a) a long period of time and spartial constant load, - b) initial time instants and arrival of wave fronts.

4.2 Layered Media

The influence of layered construction on the transient response is investigated for two different layered system. Figure 5 shows the vertical displacement response $u_{zz}(t)$ for the point with coordinates $r = 0$ (fixed) and $z = z_n$ $(n = 1, 2, 3)$. The constant hysteretic model with damping $\eta = 0.05$ is considered. In all cases, the thickness $h_i = 0.5$ $(i = 1, 2)$ and a half-space are considered. The material of the layers in each case are shown in Tab. 2.

Table 2. Multilayered media setting used.

Layer	Case A	Case B
1	Layered soil	Beryl rock
2	Beryl rock	Layered soil
half-space	Isotropic	Isotropic

In analyzing Fig. 5, the basic effect of the simple change in order of material layers is the increase or decrease of the response's amplitudes. This effect is directly related to the vertical stiffness obtained in each configuration.

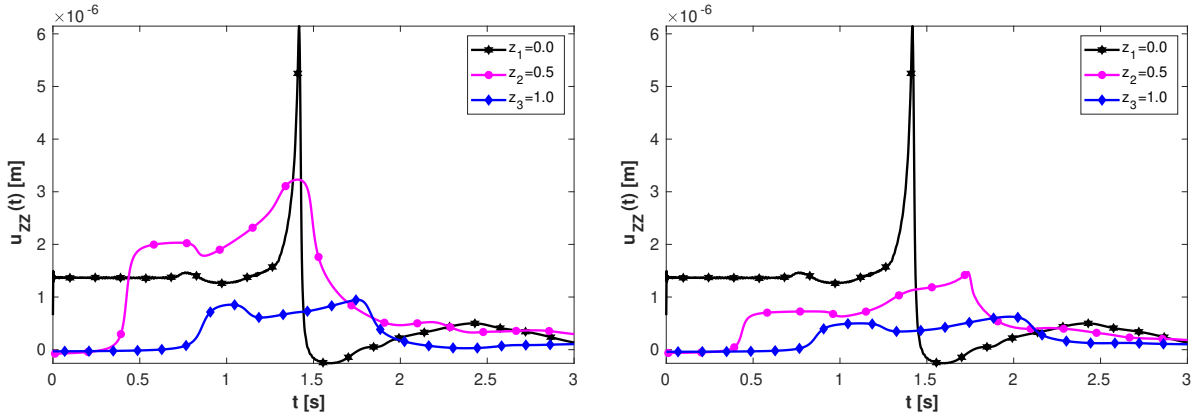

Figure 5. Transient response $u_{zz}(t)$ of - a) Case A, - b) Case B.

The transient response for different thickness (h) of the layer is shown in Fig. 6. The influence of this parameter is investigated considering a soil constituted by a layer in contact with a half-space. The vertical displacement response $u_{zz}(t)$ at the observation point with coordinates $r = 0.0$ (fixed) and $z = h$ (different thickness) are considered. All layers and the half-space are isotropic media (Tab. 1).

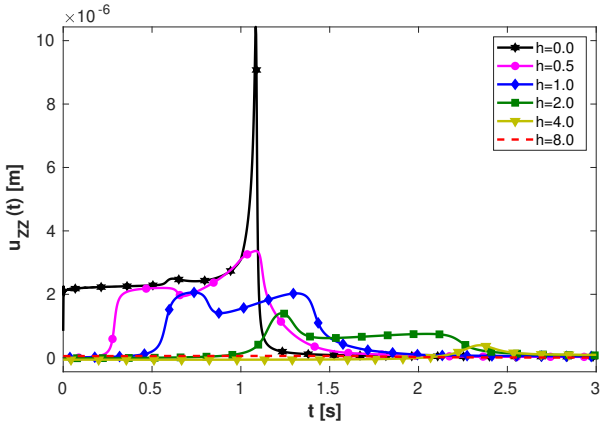

Figure 6. Effect of the layer thickness (h) on the transient response $u_{zz}(t)$.

As can be seen in Figure 6, for a deeper layers the path that must be traveled by the waves from the source point to the field point increases. Consequently, the waves have smaller amplitudes, due larger geometric and internal energy dissipation.

Figure 7 shows the influence of the damping parameter on the transient response. The constant hysteretic model with damping coefficients $\eta = 0.05$, 0.10, and 0.20 are considered. This case considers a soil constituted by a layered soil (layer) in contact with an isotropic (half-space) media. The results show the surface of the soil ($r, z = 0.0$) and the layer interface ($r = 0.0$ and $z = 0.5$) displacements. As expected, the increase of the damping leads to smaller displacement amplitudes.

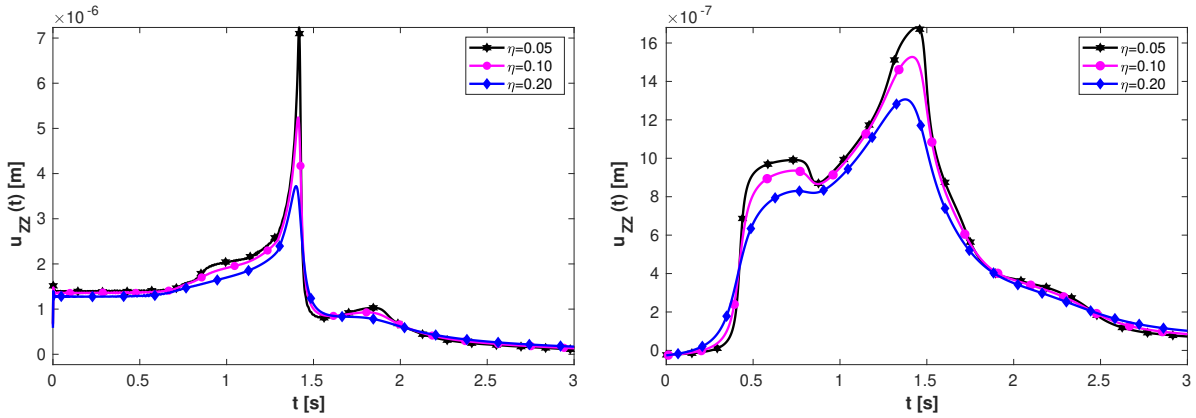

Figure 7. Transient response $u_{zz}(t)$ as function of the damping coefficient in the - a) surface ($z_n = 0.0$), - b) interface ($z_n = 0.5$).

5 Conclusions

This work investigated transient solutions for a multilayered transversely isotropic half-space subjected to an axisymmetric load on its surface. The results synthesized by numerical scheme formed by the contour deformation path method for the singular interval together with robust series extrapolation through the ϵ-algorithm with selected appropriate endpoints for the oscillatory-decaying part showed that this approach produces accurate results in very high frequencies. The long and short term transient vertical displacements response of an elastic isotropic half-space case was determined and described in terms of the wave fronts associated with compression, shear and Rayleigh waves. The transient propagation phenomena were investigated in terms of the influence of the material, layer thickness and damping parameters for the layered media.

Acknowledgements. The research leading to this article has been funded in party by the São Paulo Research Foundation - Fapesp, through grand 2017/01450-0. The support of Capes, CNPq, and Faepex-Unicamp is also gratefully acknowledged.

Authorship statement. The authors hereby confirm that they are the sole liable persons responsible for the authorship of this work, and that all material that has been herein included as part of the present paper is either the property (and authorship) of the authors, or has the permission of the owners to be included here.

References

[1] M. Adolph, E. Mesquita, and E. Romanini. A methodology to determine the transient response of the structures interacting with visco-elastic soils using the fft algorithm. In *XXI Iberian-Latin American Congress on Computational Methods in Engineering*, 2001.

[2] Y. Wang and R. K. N. D. Rajapakse. An exact stiffness method for elastodynamics of a layered orthotropic half-plane. *Journal of Applied Mechanics*, vol. 61, n. 2, pp. 339–348, 1994.

[3] R. K. N. D. Rajapakse and Y. Wang. Green's functions for transversely isotropic elastic half space. *Journal of Engineering Mechanics-asce*, vol. 119, n. 9, pp. 1724–1746, 1993.

[4] J. Labaki, E. Mesquita, and R. K. N. D. Rajapakse. Vertical vibrations of an elastic foundation with arbitrary embedment within a transversely isotropic, layered soil. *Cmes-computer Modeling in Engineering and Sciences*, vol. 103, n. 5, pp. 281–313, 2014.

[5] D. M. Barnett, J. Lothe, S. S. Gavazza, and M. J. P. Musgrave. Considerations of the existence of interfacial (stoneley) waves in bonded anisotropic elastic half-spaces. *Proceedings of the royal society of London, series A : mathematical and physical sciences*, vol. 402, n. 1822, pp. 153–166, 1985.

[6] D. M. Barnett. Bulk, surface, and interfacial waves in anisotropic linear elastic solids. *International Journal of Solids and Structures*, vol. 37, pp. 45–54, 2000.

[7] S. V. Kuznetsov. Love waves in layered anisotropic media. *Journal of Applied Mathematics and Mechanics*, vol. 70, n. 1, pp. 116–127, 2006.

[8] I. Cavalcante and J. Labaki. Correlation between physical wavenumbers and singularities in the integrand of green's functions for layered media. In *MECSOL 2019*, 2019a.

[9] L. F. Ye, K. Xiao, L. Qiu, S.-L. Chai, and J.-J. Mao. An efficient method for the computation of mixed potential green's functions in cylindrically stratified media. *Progress In Electromagnetics Research*, vol. 125, pp. 37–53, 2012.

[10] K. C. Durbhakula, A. M. Hassan, D. Chatterjee, and M. S. Kluskens. Evaluation of sommerfeld integrals using contour deformation paths for nano and microstrip antenna applications. In *2017 IEEE Applied Electromagnetics Conference (AEMC)*, 2017.

[11] I. C. Geraldo. Integração numérica de funções de green para meios estratificados. Master's thesis, Universidade Estadual de Campinas, Faculdade de Engenharia Mecânica, Campinas, 2019.

[12] I. Cavalcante and J. Labaki. Numerical integration of green's functions for layered media: a case study. In *XL Iberian-Latin American Congress on Computational Methods in Engineering*, 2019b.

[13] P. Wynn. On a device for computing the and m (s n) transformation. *Mathematical Tables and Other Aids to Computation*, vol. 10, n. 54, pp. 91, 1956.

[14] K. A. Michalski and J. R. Mosig. Efficient computation of sommerfeld integral tails – methods and algorithms. *Journal of Electromagnetic Waves and Applications*, vol. 30, n. 3, pp. 281–317, 2016.

[15] R. M. Christensen. *Theory of Viscoelasticity*. Elsevier, 1982.

[16] M. Adolph, E. Mesquita, and E. Romanini. Transient response of rigid foundations resting on viscoelastic layer. In *16th ASCE Engineering Mechanics Conference*, pp. 16–18. Citeseer, 2003.

[17] E. Mesquita, M. Adolph, P. A. Barros, and E. Romanini. Transient green and influence functions for plane strain visco-elastic half-spaces. In *Proc. IABEM SYMPOSIUM*, pp. 28–31, 2002.

[18] Y. Wang. *Fundamental solutions for multi-layered transversely isotropic elastic media and boundary element applications*. PhD thesis, University of Manitoba, Winnipeg, 1992.